Reprinted from March 1989, Vol. 111, Journal of Applied Mechanics

J. M. Powers
Visiting Assistant Professor,
Department of Mechanical and
Industrial Engineering.

D. S. Stewart
Associate Professor,
Department of Theoretical and
Applied Mechanics.

Herman Krier
Professor,
Department of Mechanical and
Industrial Engineering,
Mem. ASME

University of Illinois at
Urbana-Champaign,
Urbana, IL 61801

Analysis of Steady Compaction Waves in Porous Materials[1]

A two-phase continuum mixture model is used to analyze steady compaction waves in porous materials. It is shown that such a model admits both subsonic and supersonic steady compaction waves in response to a piston-driven boundary condition when a Tait equation is used to describe a solid matrix material and a generic static compaction relation is used to describe collapse of the matrix. Parameters for the Tait equation are chosen to match shock and compaction wave data. The model is able to predict compaction wave speed, final pressure, and final volume fraction in porous HMX. The structure of the compaction wave is also studied. A shock preceding the compaction wave structure is predicted for compaction waves travelling faster than the ambient sound speed of the solid. For subsonic compaction waves no leading shock is predicted. The compaction zone length is studied as a function of initial volume fraction, piston velocity, and compaction viscosity.

Introduction

It has been established by experiments with granular high energy solid propellants (Bernecker and Price, 1974; Price and Bernecker; 1975) and by numerical solution of unsteady two-phase reactive flow models (Bulter and Krier, 1986; Baer and Nunziato; 1986) that deflagration to detonation transition (DDT) in a confined column of such granular energetic material involves material compaction and heat release. In many cases the origin of such a DDT can be traced to the influence of a compaction wave, defined as a propagating disturbance of the solid volume fraction of the granular material. Steady compaction waves in porous HMX (cyclic nitramine) were observed by Sandusky and Liddiard (1985) and Sandusky and Bernecker (1985) arising from the impact of a constant velocity piston (piston velocity < 300 m/s). Compaction waves in these experiments travel at speeds less than 800 m/s, well below the ambient solid sound speed, which is near 3000 m/s. To understand compaction waves it is necessary to explain why this nonclassical result is obtained.

The first step in modeling compaction waves is to study steady compaction waves. With understanding gained from steady waves, it is easier to understand the time-dependent development of a compaction wave and how such a compaction wave can further evolve into a detonation wave. Although it is possible to numerically solve the coupled unsteady partial differential equations which model such dynamic compaction processes (including the formation of shock waves) (Krier and Stewart, 1985), it is difficult to interpret from such models what physical properties dictate the speed, pressure changes, and porosity changes of compaction waves. It is the goal of this paper to provide a simple method to predict these parameters as a function of material properties with a representative model.

We simulate the experiments of Sandusky and Liddiard by studying steady solutions to two-phase flow model equations. Without considering wave structure, Kooker (1986) has used an algebraic end state analysis to predict compaction wave speed as a function of piston velocity for full two-phase model equations. It is possible to extend this analysis in the limit where the effect of one of the phases is dominant. This approach was first used by Baer (1988) in his study of steady compaction wave structure. Here we provide a more detailed discussion of steady structure and basic parameter dependencies. Throughout this paper, we will compare our assumptions and results to those of Baer.

Our results show a continuous dependence of compaction wave structure with supporting piston velocity; depending on the piston velocity, two broad classes of compaction zone structure exist. At low piston velocities the compaction wave travels at speeds less than the ambient solid sound speed. We call such waves subsonic compaction waves. The structure is characterized by a smooth rise in pressure from the ambient to a higher pressure equal to the static pore collapse stress level. Subsonic compaction waves have been observed in experiment (though compaction zone widths have not been measured) and predicted by Baer. Above a critical piston velocity the compaction wave travels at speeds greater than the ambient solid sound speed. A discontinuous shock wave leads a relaxation zone where the pressure adjusts to its equilibrium static pore

[1]This work was supported by the Air Force Office of Scientific Research under Grant AFOSR-85-0311 and Los Alamos National Laboratory DOE-LANL-9XR6-5128C1.

Contributed by the Applied Mechanics Division for publication in the JOURNAL OF APPLIED MECHANICS.

Discussion on this paper should be addressed to the Editorial Department, ASME, United Engineering Center, 345 East 47th Street, New York, N.Y. 10017, and will be accepted until two months after final publication of the paper itself in the JOURNAL OF APPLIED MECHANICS. Manuscript received by ASME Applied Mechanics Division, July 10, 1987; final revision, March 8, 1988.

collapse value. We call such waves supersonic compaction waves. Supersonic compaction waves with leading shocks have not been observed nor predicted in previous studies.

A shock wave in compaction wave structure is admitted because the model equations are hyperbolic. Our model ignores the effects of diffusive momentum and energy transport. If included, these effects would define the width of the shock structure. Here it is assumed that the length scales on which these processes are important are much smaller than the relaxation scales which define compaction zone structure.

As mentioned by a reviewer, compaction wave phenomena predicted here have analogies in gas dynamics. As described by Becker and Bohme (1969), gas dynamic models which include thermodynamic relaxation effects predict a dispersed wave to result from the motion of a piston into a cylinder of gas. Steady solutions with and without discontinuous jumps are identified. These solutions have features which are similar to those predicted by our compaction wave model.

Here we comment on the differences and similarities of the original Baer study and the present study. We have relaxed Baer's incompressibility assumption and assume a fully compressible solid. We give a complete characterization of compaction wave structure as a function of piston speed including an analysis of the supersonic case. With our analysis many new results are obtained. We obtain a unique algebraic equilibrium condition for a generic static pore collapse function. As does Baer, we demonstrate that the problem of determining compaction wave structure can be reduced to solving one ordinary differential equation for volume fraction. We show that other thermodynamic quantities (pressure, density, etc.) are algebraic functions of volume fraction. An analytic solution in the strong shock limit is given.

Compaction Wave Model

We write two-phase continuum mixture equations to describe the motion of a mixture of solid particles and gas. The model, discussed in more detail by Powers, Stewart, and Krier (1987), describes two-phase flow with interphase mass, momentum, and energy transport. A density, ρ_i; pressure, P_i; energy, e_i; temperature, T_i; velocity, u_i; and volume fraction, ϕ_i, is defined for each phase (for the gas $i=1$, for the solid $i=2$). We define the volume fraction as the ratio of the volume of a constituent to the total volume. It is assumed that at each point in space both phases simultaneously exist; each phase may possess a distinct pressure, velocity, temperature, etc. For each phase mass, momentum, and energy evolution equations are written. A thermal and caloric state relation is assumed for each phase. To close the system, a compaction equation similar to that of Baer and Nunziato is utilized. The compaction equation models the time-dependent pore collapse of a porous matrix and is based on the dynamic pore collapse theory of Carroll and Holt (1972). Details about the rationale for the model are given by Baer and Nunziato and Gokhale and Krier (1982). Compaction work is assumed to be negligible.

Unsteady Model. The unsteady two-phase equations are

$$\frac{\partial}{\partial t}(\rho_i\phi_i)+\frac{\partial}{\partial x}(\rho_i\phi_i u_i)=A_i \tag{1}$$

$$\frac{\partial}{\partial t}(\rho_i\phi_i u_i)+\frac{\partial}{\partial x}(P_i\phi_i+\rho_i\phi_i u_i^2)=B_i \tag{2}$$

$$\frac{\partial}{\partial t}(\rho_i\phi_i[e_i+u_i^2/2])+\frac{\partial}{\partial x}(\rho_i\phi_i u_i[e_i+u_i^2/2+P_i/\rho_i])=C_i \tag{3}$$

$$\frac{\partial\phi_2}{\partial t}+u_2\frac{\partial\phi_2}{\partial x}=\frac{\phi_1\phi_2}{\mu_c}(P_2-P_1-f(\phi_2)) \tag{4}$$

$$P_i=P_i(\rho_i,T_i) \tag{5}$$

$$e_i=e_i(P_i,\rho_i) \tag{6}$$

$$\phi_1+\phi_2=1. \tag{7}$$

Equations (1), (2), and (3) describe the evolution of mass, momentum, and energy, respectively, of each phase. Interphase transport is represented in these equations by the terms A_i, B_i, and C_i, which are assumed to be algebraic functions of P_i, u_i, ρ_i, etc. These terms are specified such that the following conditions hold:

$$\sum_{i=1}^{2}A_i=0,\quad \sum_{i=1}^{2}B_i=0,\quad \sum_{i=1}^{2}C_i=0. \tag{8}$$

This insures that the mixture equations obtained by adding the constituent mass, momentum, and energy equations are conservative.

For each phase we define an initial temperature, density, velocity, and volume fraction. The subscript 0 is taken to represent an initial condition.

$$T_i=T_{i0},\quad \rho_i=\rho_{i0},\quad u_{i0}=0,\quad \phi_2=\phi_{20} \tag{9}$$

Other variables are determined by the algebraic relations (5), (6), and (7).

Equation (4) is the compaction equation. A similar model equation has been used by Butcher, Carroll, and Holt (1974) to describe time-dependent (dynamic) pore collapse in porous aluminum. The parameter μ_c is defined as compaction viscosity, not to be confused with the viscosity associated with momentum diffusion. The compaction viscosity defines the only length scale in this problem. The existence of such a parameter is still a modeling assumption and its value has not been measured. There is, however, a theoretical justification for the dynamic pore collapse model. It has been shown (Baer and Nunziato) that when dynamic compaction is incorporated into two-phase model equations, the equations are hyperbolic. We require the initial value problem to be hyperbolic in order to insure a stable solution.

In the compaction equation (4) f represents the intragranular stress in the porous medium. It is assumed to be a function of the volume fraction. Baer has estimated f from Elban and Chiarito's (1986) empirical quasi-static data obtained by measuring the static pressure necessary to compact a porous media to a given volume fraction. Carroll and Holt have suggested an analytical form for f for three regimes of pore collapse, an elastic phase, an elastic-plastic phase, and a plastic phase. In this work we will model f with an equation similar to Carroll and Holt's plastic phase equation. Here we make two *a priori* assumptions about f. First, we assume f is a monotonically increasing function of volume fraction so that an increasing hydrostatic stress is necessary to balance the increased intragranular stress which arises due to an increasing solid volume fraction. Second, we assume that at the initial state f must equal the difference of the solid and gas pressures so that the system is initially in equilibrium. Our results show that with these assumptions, compaction wave phenomena are relatively insensitive to the particular functional form of f.

Equations (5) and (6) are state relations for each phase. Equation (7) arises from the definition of volume fraction. It states that all volume is occupied by either solid or gas. Using standard techniques it can be shown that these equations are hyperbolic; thus, initial value problems are well posed. The characteristic wave speeds are u_1, u_2, $u_1\pm c_1$, and $u_2\pm c_2$, where c_i represents the sound speed of phase i.

Dimensionless Steady Model. To study compaction waves in the context of this model, we make the following assumptions: (1) a steady wave travelling at speed D exists, (2) gas phase equations may be neglected, (3) interphase transport

terms may be neglected, and (4) the solid phase is described by a Tait equation of state. As a result of Assumption 1, equations (1) through (4) may be transformed to ordinary differential equations under the Galilean transformation $\xi = x - Dt$, $v = u - D$. By examining the dimensionless form of equations (1) through (7), it can be shown that in the limit as the ratio of initial gas density to initial solid density goes to zero, that we are justified in neglecting gas phase equations and interphase transport. To prove this contention, one can integrate the steady mixture mass, momentum, and energy equations formed by adding the component equations to form algebraic mixture equations. By making these equations dimensionless (as shown by Powers, Stewart, and Krier), it is seen that all gas phase quantities are multiplied by the density ratio ρ_{10}/ρ_{20}. As long as dimensionless gas phase properties are less than $O(\rho_{20}/\rho_{10})$, we are justified in neglecting the effect of the gas phase.

As the gas phase is neglected, the subscripts 1 and 2 are discarded. All variables are understood to represent solid phase variables. The caloric Tait equation (Bdzil et al., 1981) for the solid is

$$e = \frac{P + \rho_0 s}{(\gamma - 1)\rho}. \tag{10}$$

Here γ and s are parameters that define the Tait state equation. The value of γ is chosen to match shock Hugoniot data (Marsh, 1980). It is analogous to the specific heat ratio for an ideal equation of state. We define s as the nonideal solid parameter. In this study we view s as an adjustable parameter which allows us to vary the equation of state in a simple way in order to show how the results are sensitive to nonideal state effects. When $s = 0$, the state equation is an ideal state equation. For this study a value of s was chosen to match the compaction wave data of Sandusky and Liddiard.

To determine the ambient solid sound speed, an important term in this analysis, it is necessary to specify a thermal equation of state. By assuming a constant specific heat at constant value c_v, a thermal equation of state consistent with equation (10) can be derived:

$$P = (\gamma - 1)c_v \rho T - \rho_0 s/\gamma. \tag{11}$$

Based on equations (10) and (11) an equation for the solid sound speed c is easily derived by using the thermodynamic identity $Td\eta = de - P/\rho^2 d\rho$, where η is the entropy.

$$c^2 = \frac{\partial P}{\partial \rho}\bigg|_{\eta} = \gamma(\gamma - 1)c_v T \tag{12}$$

To simplify the analysis, dimensionless variables are denoted by an asterisk subscript and are defined as follows

$$\rho_* = \rho/\rho_0,\ v_* = v/D,\ e_* = e/D^2,\ T_* = c_v T/D^2,$$
$$P_* = P/(\rho_0 D^2),\ \xi_* = \xi \rho_0 D/\mu_c.$$

With this choice of dimensionless variables four dimensionless parameters arise.

γ = Tait Solid Parameter, $\quad \dfrac{s}{D^2\gamma} = \sigma$ = Nonideal Solid Parameter

$$\frac{\gamma(\gamma - 1)c_v T_0 - s}{\gamma D^2} = \pi = \text{initial pressure},$$

ϕ_0 = initial volume fraction

For materials of interest ϕ_0 and γ are of order 1. Interesting limiting cases can be studied when $s \to 0$, corresponding to the strong shock or weak nonideal effect limit, or when $\pi \to 0$, corresponding to the strong shock limit.

With the assumptions made, we can write steady dimensionless equations to describe the compaction of an inert solid porous material as follows:

$$\frac{d}{d\xi_*}(\rho_* \phi v_*) = 0 \tag{13}$$

$$\frac{d}{d\xi_*}(P_* \phi + \rho_* \phi v_*^2) = 0 \tag{14}$$

$$\frac{d}{d\xi_*}(\rho_* \phi v_* [e_* + v_*^2/2 + P_*/\rho_*]) = 0 \tag{15}$$

$$\frac{d\phi}{d\xi_*} = \frac{\phi(1 - \phi)}{v_*}(P_* - f_*(\phi)) \tag{16}$$

$$e_* = \frac{P_* + \gamma\sigma}{(\gamma - 1)\rho_*}. \tag{17}$$

Initial conditions are specified as

$$\rho_* = 1,\ \phi = \phi_0,\ v_* = -1,\ P_* = \pi. \tag{18}$$

Equations (13)–(17) are equivalent to Baer's steady model except a term Baer calls "compaction work" is not included and a simpler state equation is used. Equations (13), (14), and (15) may be integrated subject to initial conditions (18) resulting in the following set of equations:

$$\frac{d\phi}{d\xi_*} = \frac{\phi(1 - \phi)}{v_*}(P_* - f_*(\phi)) \tag{19}$$

$$\rho_* \phi v_* = -\phi_0 \tag{20}$$

$$P_* \phi + \rho_* \phi v_*^2 = \phi_0(\pi + 1) \tag{21}$$

$$\rho_* \phi v_* (e_* + v_*^2/2 + P_*/\rho_*) = -\phi_0 \left(\frac{\pi + \gamma\sigma}{\gamma - 1} + 1/2 + \pi\right) \tag{22}$$

$$e_* = \frac{P_* + \gamma\sigma}{(\gamma - 1)\rho_*} \tag{23}$$

From equations (20) through (23), equations for pressure and velocity as functions of volume fraction can be written. Equation (23) is used to eliminate energy from equation (22). Velocity is eliminated from equations (21) and (22) by using equation (20). Then density is eliminated from equation (22) by using equation (21). What remains is a quadratic equation involving only pressure and volume fraction. It is possible to solve this equation for pressure explicitly in terms of volume fraction. The solution is

$$P_* = \frac{\phi_0}{\phi(\gamma + 1)}\left(\frac{\gamma\sigma\phi}{\phi_0} - 1 - \pi\right).$$
$$\left[-1 \pm \sqrt{1 + \frac{(\gamma + 1)\left[2\gamma\sigma\left(\frac{\phi}{\phi_0}(1 + \pi) - 1\right) - \pi(2 - \pi(\gamma - 1))\right]}{\left(\frac{\gamma\sigma\phi}{\phi_0} - 1 - \pi\right)^2}}\right]. \tag{24}$$

The solution corresponding to the positive branch is the physically relevant one. The negative branch is associated with negative pressure. Equations (20) and (21) may be simultaneously solved for velocity as a function of pressure and volume fraction. The velocity is given by

$$v_* = \frac{P_* \phi - \phi_0(1 + \pi)}{\phi_0}. \tag{25}$$

By using equation (24) to substitute for pressure in equation (25), velocity is available as a function of volume fraction alone. The mass equation (20) can be used to give density as a function of volume fraction and then the state equation (17) can be used to give energy as a function of volume fraction.

Thus all variables in the compaction equation (19) can be expressed as functions of volume fraction; the compaction wave problem is reduced to solving one ordinary differential equation (19) for volume fraction subject to the condition $\phi = \phi_0$ at $\xi = 0$.

Next we describe the technique for determining wave speed as a function of piston velocity. This calculation is algebraic and can be made without regard to structure. The solution is parameterized by the wave velocity through the definitions of π and σ. Instead of using a piston velocity as an input condition, it is easier to consider the wave speed to be known and from that wave speed calculate a piston velocity. By assuming static pressure equilibrium end state in equation (19) $(P_*(\phi) = f_*(\phi))$, it is possible to determine the equilibrium volume fraction and thus, from equations (24) and (25), the final velocity v_*. The piston velocity (u_p) is found by transforming the final velocity to the lab frame by using the transformation $u_p = D(v_* + 1)$.

Pressure equilibrium end states are found when a volume fraction is found such that the pressure given by equation (24) matches the intragranular stress predicted by f. In the initial state, equation (24) predicts a pressure of π, the dimensionless initial pressure. But assumption f also yields a value of π in the initial state so that the undisturbed material is stationary. In Fig. 1, dimensional pressure in HMX is plotted as a function of volume fraction from equation (24) for a series of wave speeds and an initial volume fraction of 0.73. Parameters used to model HMX are listed in Table 1. (We use c_v, μ_c, and ρ_0 of Baer and Nunziato and estimate the parameters γ and s from shock and compaction data.) All curves pass through the point of initial pressure and volume fraction.

Table 1 HMX Material Properties and Initial Conditions

Parameter	Description	Value
γ	Tait Solid Parameter	5
c_v	Constant Volume Specific Heat	1500 J/(kg K)
s	Nonideal Solid Parameter	8.976×10^6 m^2/s^2
T_0	Initial Temperature	300 K
ρ_0	Initial Density	1900 kg/m^3
μ_c	Compaction Viscosity	1000 kg/(ms)

The curve on Fig. 1 for the ambient sonic wave speed ($D = 3000$ m/s) has a special property whose importance will be apparent in the following paragraph. For this curve a volume fraction minimum exists at the initial volume value. It can be proven for a sonic wave speed, that the discriminant in equation (24) is identically zero for $\phi = \phi_0$ and $D = \gamma(\gamma - 1)\, c_v T_0$ (the ambient solid sonic wave speed).

The positive pressure branch of equation (24) is a double-valued function of volume fraction for wave velocities that exceed the ambient solid sound speed and single-valued for wave velocities less than or equal to the ambient solid sound speed. For subsonic wave speeds, small increases from the initial volume fraction cause small positive perturbations in pressure. For supersonic wave speeds a positive increase of the initial volume fraction is only acceptable if the pressure jumps discontinuously to a shocked value of the upper portion of the double-valued $P_* - \phi$ curve. Because the governing equations are hyperbolic, these shocks jump are admissible. From equation (19) the shock jump condition for volume fraction is

$$[\phi]_0^s = 0 \tag{26}$$

where "0" denotes the initial state and "s" the shock state. Thus the shock volume fraction is always equal to the initial volume fraction.

From equations (24) and (25) the shock pressure and particle velocity can be determined. The shocked values are independent of the initial solid volume fraction.

$$P_s = \frac{2 - (\pi + \sigma)(\gamma - 1)}{\gamma + 1} - \sigma \tag{27}$$

$$v_s = -\frac{(\gamma - 1) + 2\gamma(\pi + \sigma)}{\gamma + 1}\,. \tag{28}$$

The combination of parameters $\pi + \sigma$ is independent of the nonideal solid parameter s. So from equations (27) and (28) it is deduced that nonideal effects lower the shock pressure by a constant, σ, and do not affect the shock particle velocity.

Based on the implications of equation (24), the structure analysis is thus conveniently split in two classes, subsonic and supersonic. As wave speed increases from subsonic values, the initial pressure at the wave front is the ambient pressure until

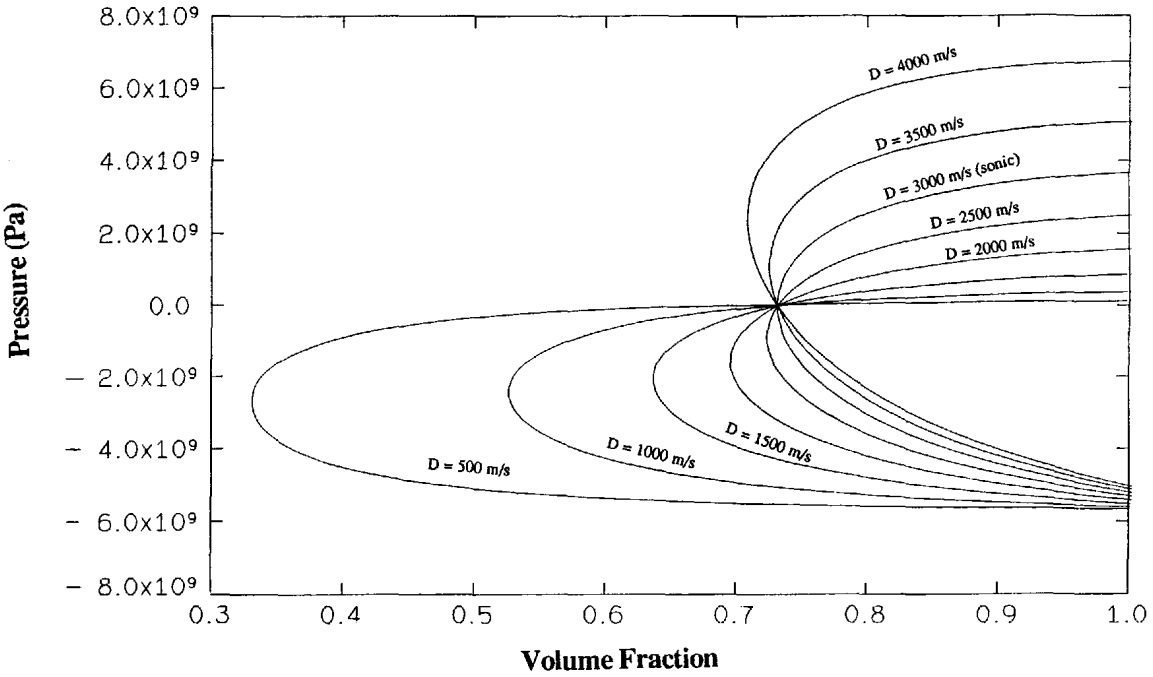

Fig. 1 Pressure versus volume fraction from conservation and state equations for subsonic, sonic, and supersonic wave speeds

the compaction wave speed is sonic. For wave speed greater than the ambient solid sound speed the initial pressure jumps are dictated by equation (27). A plot of the leading pressure versus compaction wave speed is shown in Fig. 2.

As an aside, we note that a criterion for a solid equation of state is that the candidate equation along with the Rankine-Hugoniot jump conditions be able to match experimental piston impact data. For voidless HMX ($\phi = 1$) observations of shock wave speed as a function of piston velocity are reported by Marsh (1980). By rewriting equation (28) in dimensional form, we solve for D as a function of piston velocity.

$$D = \frac{1+\gamma}{4} u_p + \sqrt{\left(\frac{1+\gamma}{4} u_p\right)^2 + \gamma(\gamma-1)c_v T_0}. \qquad (29)$$

From equation (12), the term $\gamma(\gamma-1)c_v T_0$ is the square of the ambient sound speed for the nonideal solid. In a result familiar from gas dynamics, it can be deduced from equation (29) that the minimum steady shock wave speed admitted in response to a piston boundary condition is the ambient sonic speed. For values of γ, c_v, and T_0 listed in Table 1, we plot shock wave speed D as a function of piston velocity u_p and data from Marsh in Fig 3. We fixed γ such that there is agreement between the data and the model predictions. In the range of piston velocities shown, equation (29) approximates a linear D versus u_p relation used by other modelers to match this data.

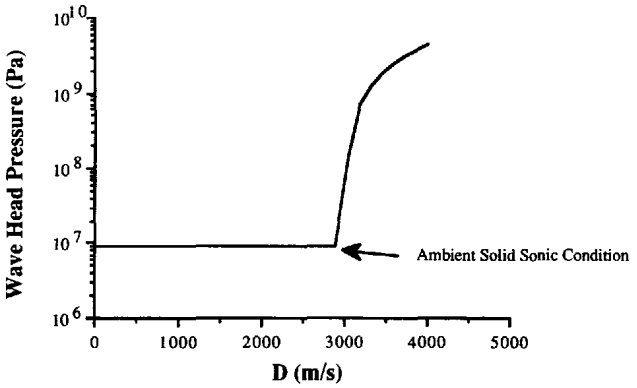

Fig. 2 Wave head pressure versus wave speed

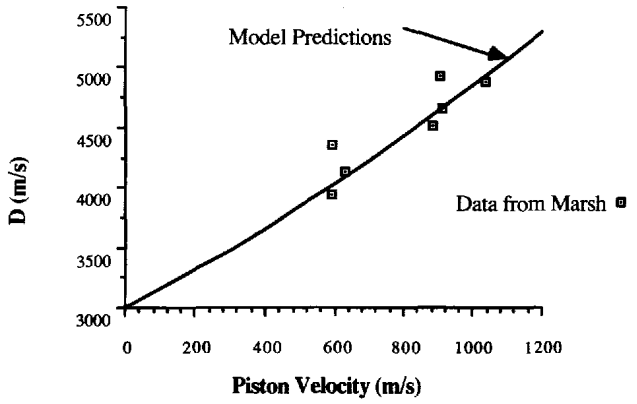

Fig.3 Predictions and observations of shock wave speed

Subsonic Compaction Waves

Subsonic End States. To study subsonic compaction waves admitted by equation (19), we choose a form for f_*:

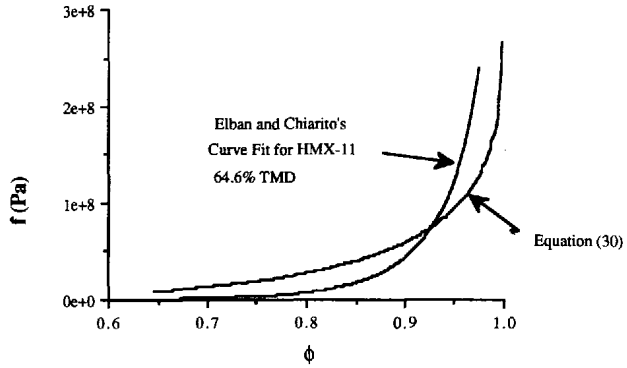

Fig. 4 Comparison of Elban's static pore collapse data with equation (30)

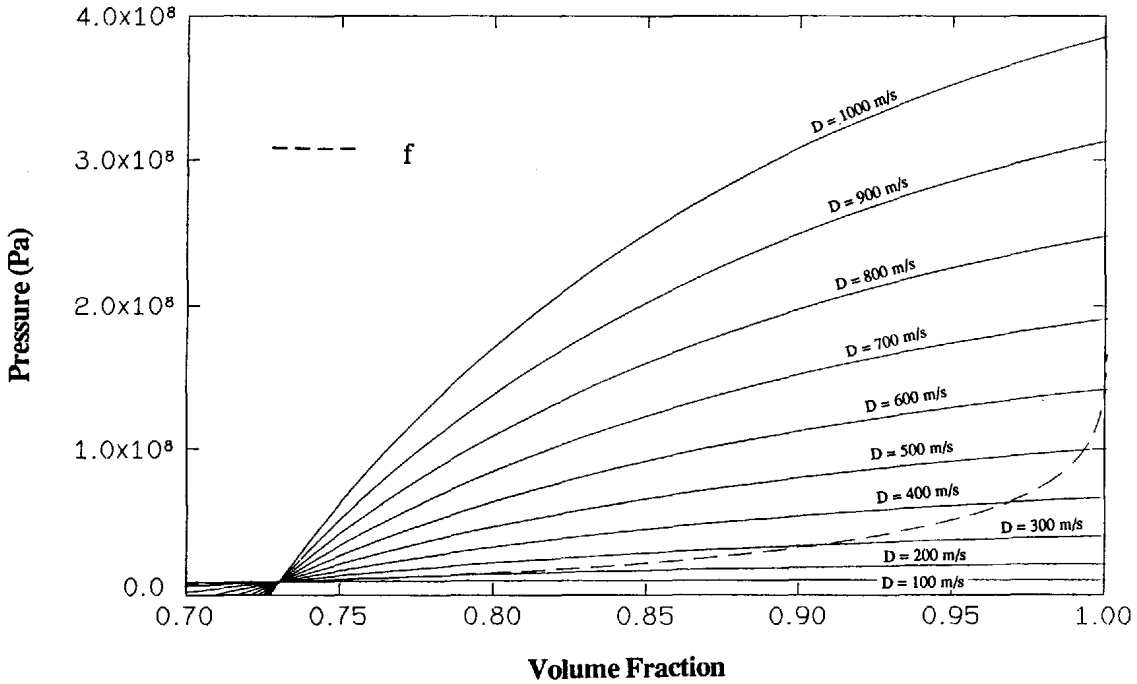

Fig. 5 Pressure versus volume fraction from conservation and state equations for subsonic wave speeds and static pore collapse function, f

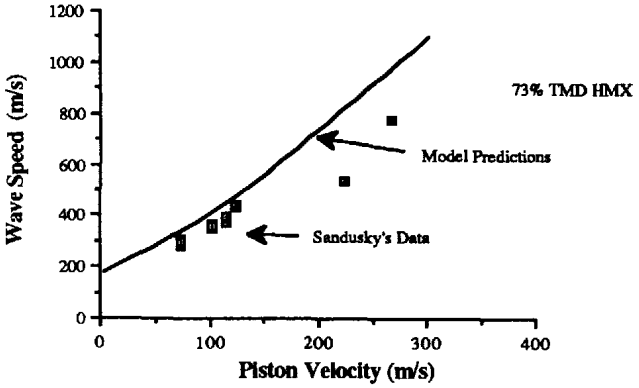

Fig. 6 Compaction wave speed versus piston velocity for subsonic compaction

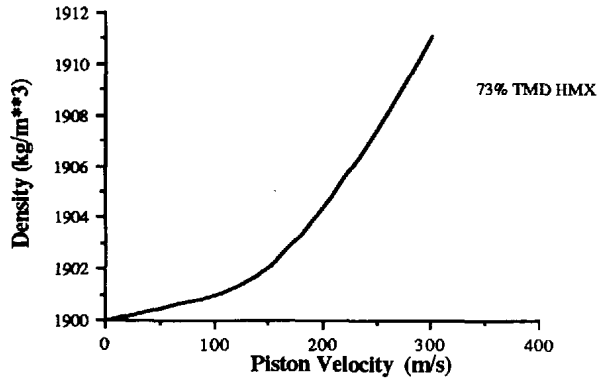

Fig. 7 Final density versus piston velocity for subsonic compaction

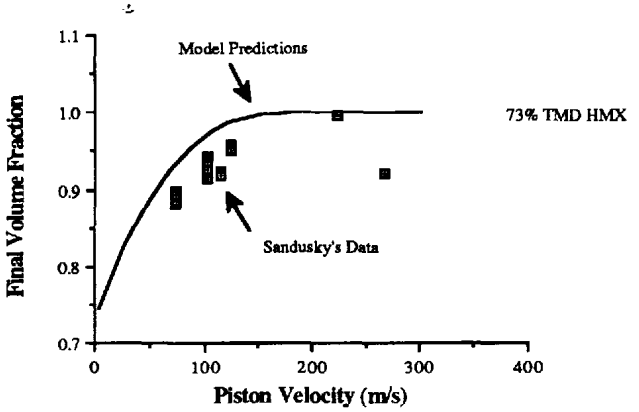

Fig. 8 Final volume fraction versus piston velocity for subsonic compaction

$$f_*(\phi) = \pi \frac{\phi^2}{\phi_0^2} \frac{(2-\phi_0)^2}{(2-\phi)^2} \frac{\ln\left[\frac{1}{1-\phi}\right]}{\ln\left[\frac{1}{1-\phi_0}\right]}. \tag{30}$$

This function satisfes the requirements described earlier, namely, it is a monotonically increasing function of volume fraction and is constructed such that the system is in equilibrium in the initial state. It has the same form as the plastic phase static pore collapse relation given by Carroll and Holt. It is not the Carroll and Holt relation as the leading coefficent in the Carroll and Holt relation is the yield stress of the solid. In equation (30) the leading coefficient is a function of initial volume fraction. Predictions of equation (30) approximately match the experimental results of Elban and Chiarito. Figure 4 compares a curve fit of Elban and

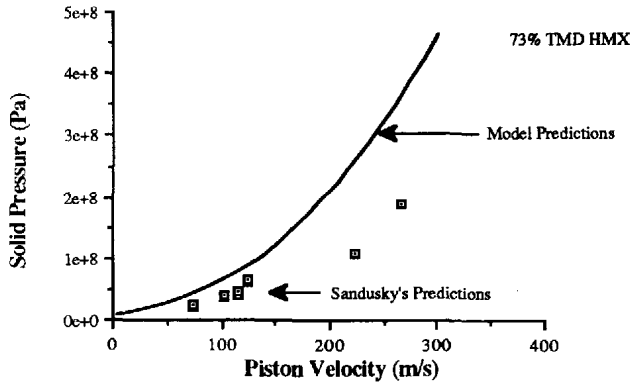

Fig. 9 Pressure versus piston velocity for subsonic compaction

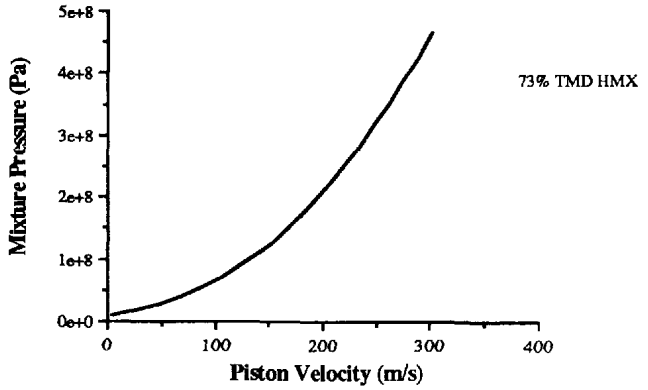

Fig. 10 Mixture pressure versus piston velocity for subsonic compaction

Chiarito's data for HMX with the approximation given by equation (30).

To locate an end state we use equations (24) and (30) to set $P_*(\phi) = F_*(\phi)$ and solve for ϕ. For 73 percent theoretical maximum density (TMD) HMX (volume fraction = 0.73) and a variety of subsonic wave speeds, curves of pressure versus volume fraction from equations (24) and (30) are plotted in Fig. 5. As wave speed increases, the final volume fraction increases. For wave speeds above 600 m/s nearly complete compaction is predicted. For wave speeds of about 200 m/s or lower, no steady compaction wave is predicted. This is solely a consequence of the assumed form of f. The form of f chosen crosses through the initial point with a positive slope and fails to intersect the pressure-volume fraction curves for low wave speeds.

For 73 percent TMD HMX Figs. 6 through 10 shows plots of compaction wave speed, final density, final volume fraction, final pressure, and final mixture pressure (mixture pressure = pressure * volume fraction) versus piston velocity. Also shown are the observations of Sandusky and Liddiard and Sandusky and Bernecker of wave speed and final volume fraction and their predictions of pressure. The relatively small density changes verify that Baer's incompressibility assumption is a good approximation. Figures 11 through 13 show predictions of compaction wave speed, final volume fraction, and final mixture pressure as a function of initial volume fraction for a constant piston velocity of 100 m/s along with Sandusky's predictions as reported by Kooker (1987).

Equation (19) has been numerically integrated to determine the structure of the subsonic compaction zone. In the numerical integrations we use pressure, velocity, and f as given by equations (24), (25), and (30), respectively. The integrations were performed on the University of Illinois at Urbana-Champaign's Cyber 175 computer using the IMSL routine DVERK. A step size was chosen such that approximately fifty points described the compaction zone. Negligible changes results from using more points. The integration was per-

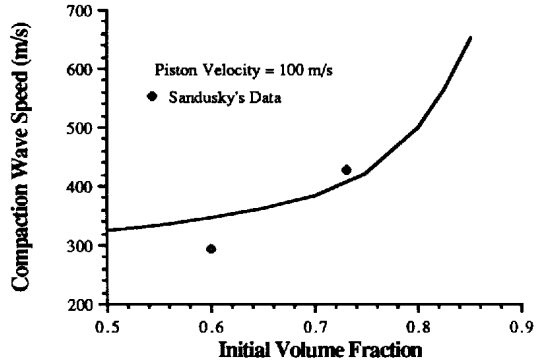

Fig. 11 Compaction wave speed versus initial volume fraction

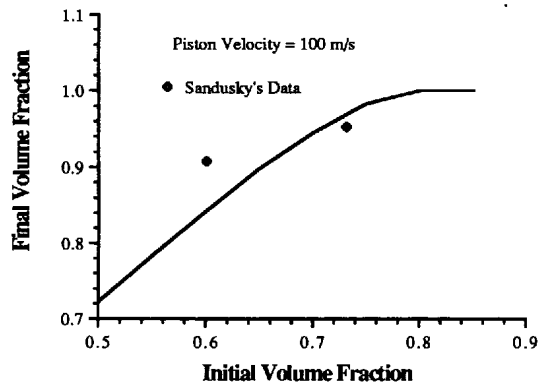

Fig. 12 Final volume fraction versus initial volume fraction

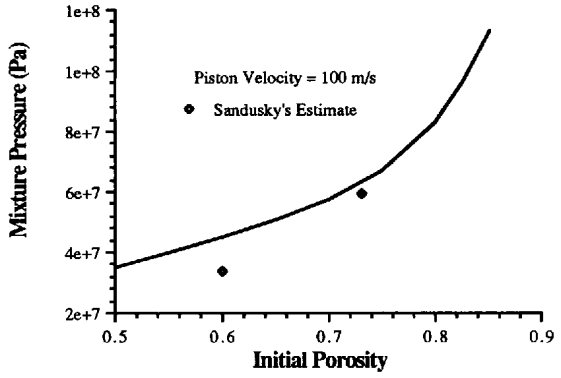

Fig. 13 Mixture pressure versus initial volume fraction

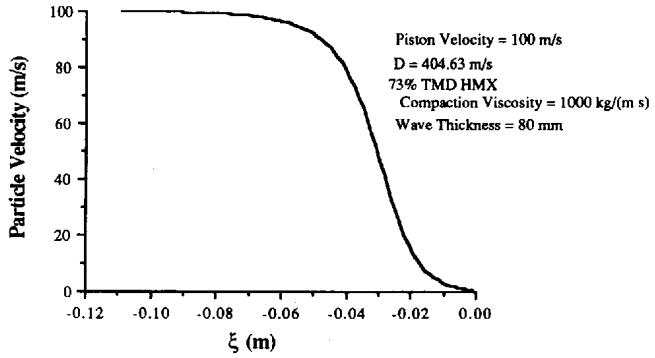

Fig. 14 Particle velocity versus distance for subsonic compaction

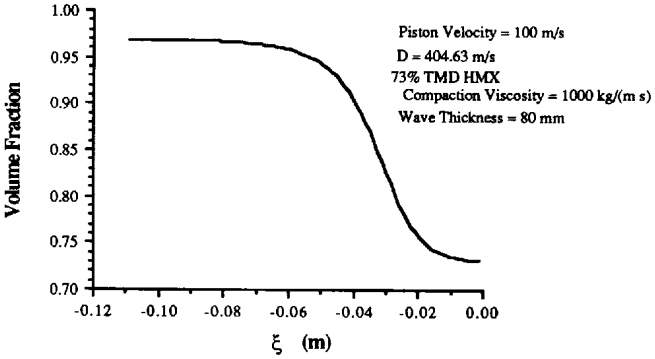

Fig. 15 Volume fraction versus distance for subsonic compaction

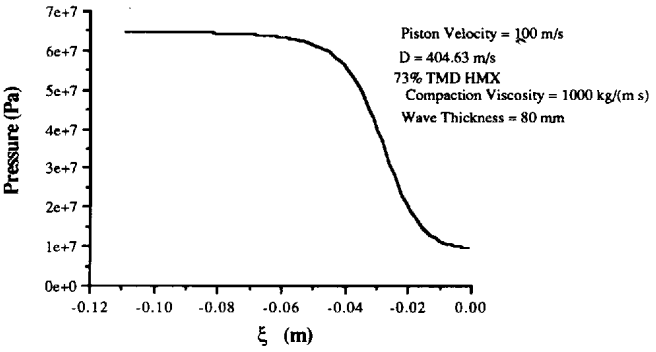

Fig. 16 Pressure versus distance for subsonic compaction

formed starting at $\xi_* = 0$ and integrating towards $\xi_* \to -\infty$. To initiate the integration, a small positive perturbation of volume fraction was introduced which, in this case, causes a small positive perturbation in pressure.

Figures 14, 15, and 16 show the particle velocity, volume fraction, and pressure in the compaction zone for a subsonic compaction wave. Here the piston velocity is 100 m/s and the initial volume fraction is 0.73. The compaction wave speed is 404.63 m/s. For an assumed compaction viscosity of 1000 kg/(ms) a compaction wave thickness of 80 mm is predicted. Because compaction viscosity defines the only length scale in this problem, compaction viscosity only serves to define the compaction wave thickness. For the same value of compaction viscosity Baer reports a compaction wave thickness of 31.9 mm. The discrepancy could be due to many effects including our definition of compaction zone length. It is important to note that the length is of the same order of magnitude. Final pressure, wave speed, and final volume fraction are unchanged by the value chosen for compaction viscosity. By measuring a compaction wave thickness, an estimate could be made for the compaction viscosity.

Supersonic Compaction Waves

End States. At 0.73 initial porosity for piston velocities greater than 884 m/s, supersonic compaction waves are also admitted. Figures 17 through 21 show plots of compaction wave speed, final density, final volume fraction, final pressure, and final mixture pressure as a function of piston velocity. These curves encompass both the subsonic and supersonic compaction wave end states. It is seen that the end states are a continuous function of piston velocity. Also plotted on Fig. 17 is the shock wave speed as a function of piston velocity. For large wave speeds the predicted shock velocity converges with the compaction wave velocity. It is demonstrated next that this is a consequence of nonideal effects having little importance at supersonic wave speeds. Furthermore, it will be demonstrated that the existence of subsonic compaction waves can be attributed solely to nonideal effects.

Supersonic Structure. Equations (24) and (25) can be simplified in the limit as $\sigma \to 0$. The limit of small σ corresponds either to negligible nonideal effects or large wave

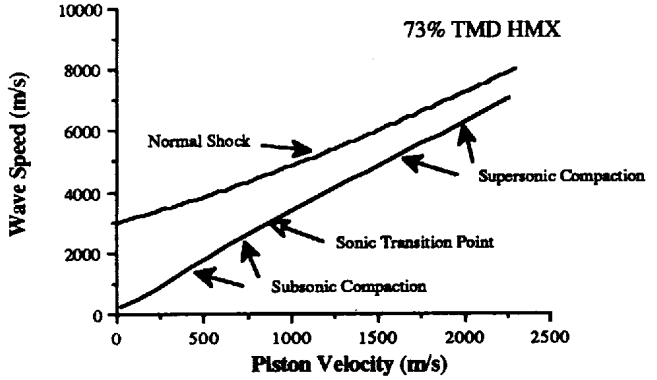

Fig. 17 Shock and compaction wave speeds versus piston velocity for subsonic and supersonic compaction

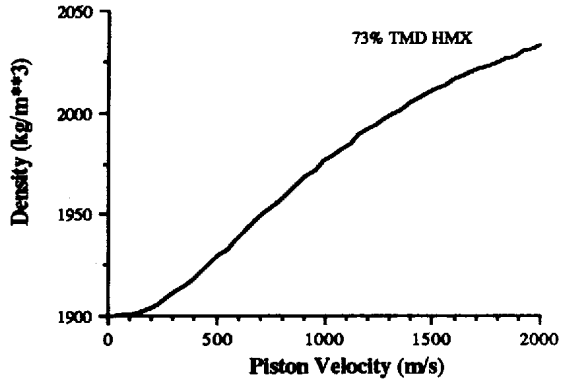

Fig. 18 Density versus piston velocity for subsonic and supersonic compaction

speed. In the limit as $\sigma \to 0$ equations (24), (25), and (19) can be written as

$$P_* = \frac{P_s \phi_0}{\phi} \tag{31}$$

$$v_* = v_s \tag{32}$$

$$\frac{d\phi}{d\xi_*} = \frac{1-\phi}{v_s}\,(P_s\phi_0 - \phi f_*(\phi)). \tag{33}$$

Equation (32) holds that in this limit the velocity is constant in the relaxation zone and is equal to the shocked particle velocity. For $s \equiv 0$ (that is for an ideal state relation) equation (32) is equivalent to equation (29); thus, for an ideal state relation the minimum compaction wave speed is the ambient sonic speed. *Any subsonic compaction wave admitted by the model (equations (19)-(23)) is a direct consequence of nonideal state effects.*

In the strong shock limit $D \to \infty$, and both π and $\sigma \to 0$. Equation (33) has a simple solution in this limit, assuming f_* to be sufficiently bounded. (Note that because of the logarithmic singularity at $\phi = 1$, (30) does not meet this criterion. We do not, however, restrict ourselves to functions of this form.) In this limit equation (33) becomes

$$\frac{d\phi}{d\xi_*} = -\frac{2\phi_0}{\gamma - 1}\,(1-\phi) \tag{34}$$

whose solution is

$$\phi = 1 - (1-\phi_0)\exp\left(\frac{2\phi_0}{\gamma-1}\,\xi_*\right). \tag{35}$$

In terms of dimensional parameters, the compaction zone thickness found by equating the exponent in equation (35) to one and substituting the expression for piston velocity for wave speed is estimated as

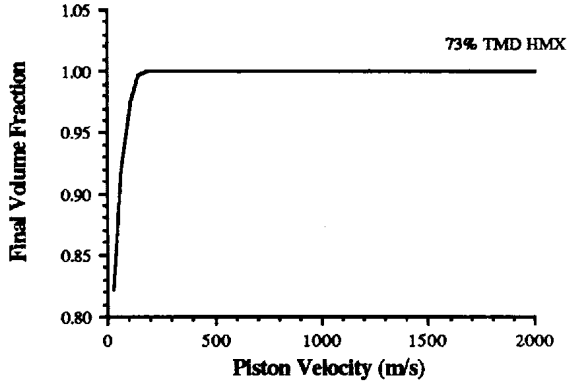

Fig. 19 Final volume fraction versus piston speed for subsonic and supersonic compaction

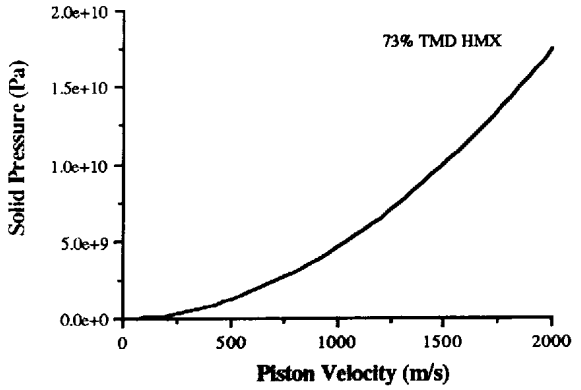

Fig. 20 Pressure versus piston velocity for subsonic and supersonic compaction

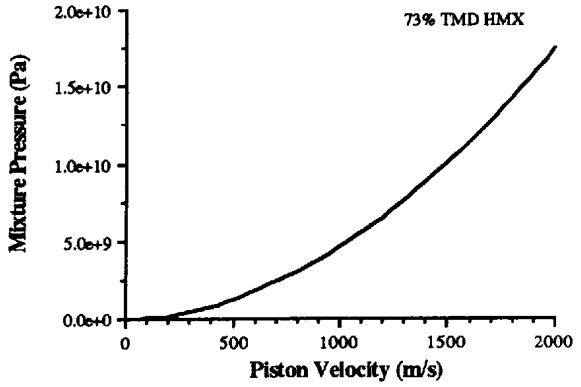

Fig. 21 Mixture pressure versus piston velocity for subsonic and supersonic compaction

$$L_{\text{comp}} = O\left(\frac{2(\gamma-1)\mu_c}{(\gamma+1)\rho_0\phi_0 u_p}\right). \tag{36}$$

The length is proportional to compaction viscosity and inversely proportional to piston velocity and the product of density and volume fraction.

An example of supersonic structure arising from the impact of a 1000 m/s piston is now given. Figures 22, 23, and 24 show the particle velocity, volume fraction, and pressure in the compaction zone for a supersonic compaction wave. Here, the initial volume fraction is 0.73. The compaction wave speed is 3353.67 m/s and the wave thickness is 2.9 mm. It is seen that pressure and particle velocity undergo shock jumps. Volume fraction does not undergo a shock jump; however, its derivative does jump at the initial point.

Compaction Zone Thickness

It is possible to study the parametric dependence of compac-

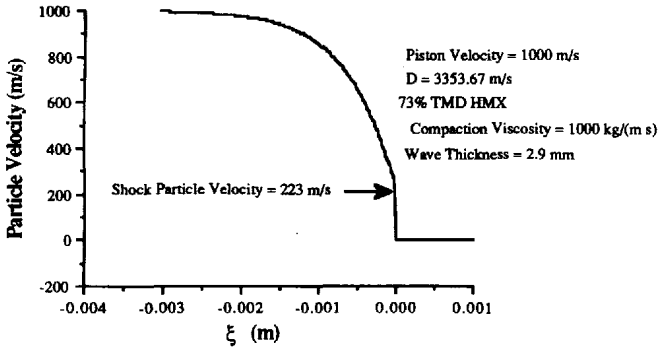

Fig. 22 Particle velocity versus distance for supersonic compaction

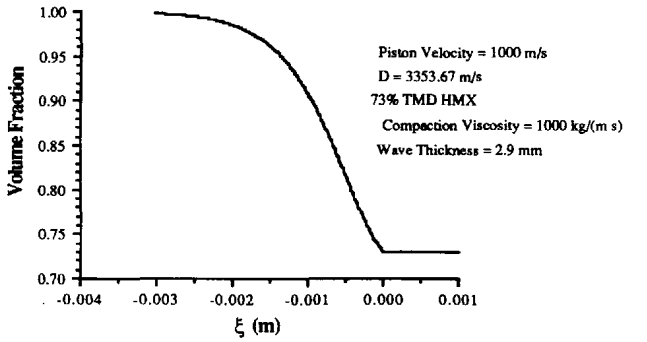

Fig. 23 Volume fraction versus distance for supersonic compaction

tion zone thickness. Given a constant compaction viscosity, our model can predict compaction zone thickness as a function of initial volume fraction and piston velocity. Should experiments be devised to measure the compaction zone thickness, the experiments could provide a means to verify the theory.

The thickness is defined as the distance at which the ratio of the difference of instantaneous volume fraction, and initial volume fraction,to the difference of final volume fraction, and initial volume fraction, is equal to 0.99. The final volume fraction is available from the algebraic end state calculation. Figure 25 shows the compaction zone length versus initial volume fraction for a piston velocity of 100 m/s and compaction viscosity of 1000 kg/(ms). We do not understand why the peak in this curve occurs. We do note that for high initial volume fraction, the zone length decreases as initial volume fraction increases in accordance with the predictions of equation (36) for supersonic compaction. We speculate that for low porosity a different mechanism dictates the subsonic compaction zone length than supersonic length. Figure 26 shows compaction zone length versus piston velocity for 73 percent TMD HMX and compaction viscosity of 1000 kg/(ms). The compaction zone length decreases with increasing piston velocity in accordance with the predictions of equation (36) for supersponic compaction. Figure 27 shows a compaction zone length as a function of compaction viscosity for a 100 m/s piston velocity and 0.73 initial volume fraction. As no estimates are available for compaction viscosity, compaction zone lengths for a wide range of compaction viscosity have been plotted. Though plotted on a log scale, the relationship is truly linear with the compaction zone length equal to a constant mutiplied by the compaction viscosity.

Discussion

The piston impact problem for a compressible porous solid has been solved in the context of a steady two-phase model

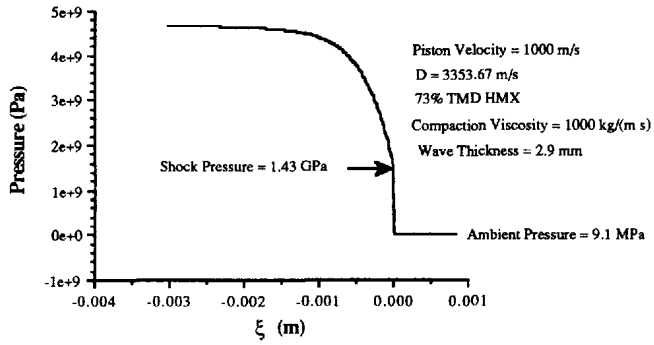

Fig. 24 Pressure versus distance for supersonic compaction

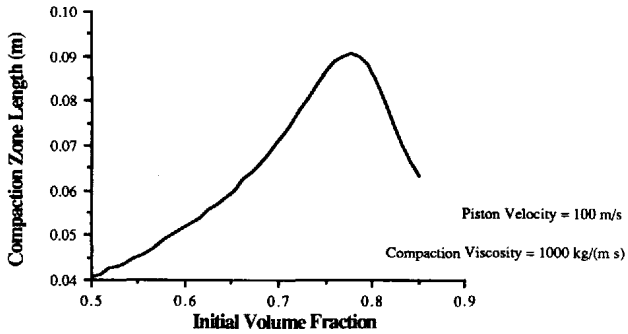

Fig. 25 Compaction zone length versus initial volume fraction

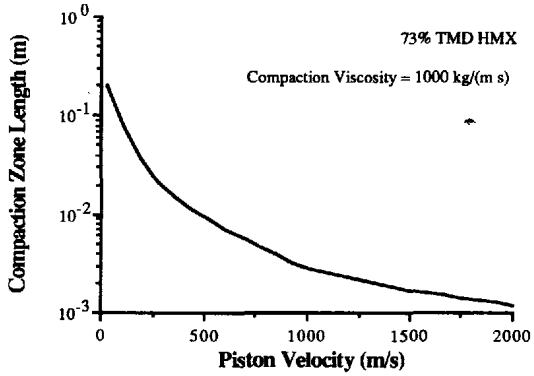

Fig. 26 Compaction zone length versus piston velocity

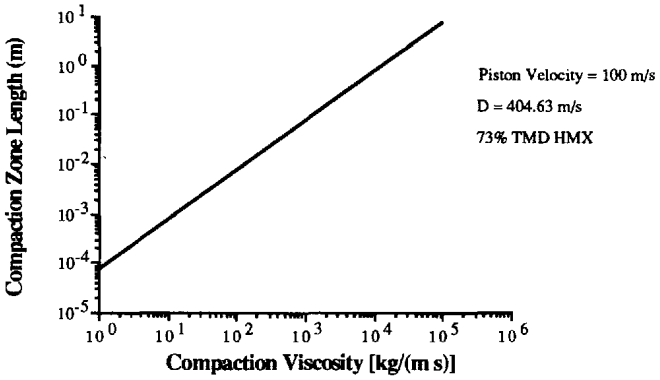

Fig. 27 Compaction zone length versus compaction viscosity

neglecting gas phase effects. With this model, it is possible to obtain an exact solution for the compaction wave speed, final porosity, and final pressure. The degree of accuracy of our predictions can be attributed to the ad hoc estimates for the nonideal solid parameter and the assumed form of the static

pore collapse function, f. We do not claim that our model is truly representative of porous HMX, only that its functional form is essentially correct. Within the framework of this model it is possible to understand the general features of a compaction wave.

As summarized by Kooker (1987), many compaction wave models do not consider dynamic pore collapse; rather, they enforce static pore collapse ($P=f$) throughout the flow field. In the context of the zero gas density limit, such as assumption results in a compaction wave without structure. The pressure discontinuously adjusts to a static equilibrium value. However, it it not established whether two-phase models with static pore collapse are hyberbolic, a necessary condition if jumps are to be admitted. For two-phase models assuming pressure equilibrium between phases but not incorporating quasi-static compaction data, Lyczkowski et al. (1978) have identified regimes in which unsteady two-phase equations are not hyperbolic.

There are many ways to extend this work. By including the effects of the gas phase, it should be possible to determine how the gas phase's presence modifies the compaction wave structure. By including the effect of particle size in f, it should be possible to model the experiments of Elban, et al. (1987) which show that the static pore collapse stress level is a function of both volume fraction and particle size. By considering the solid to be composed of particles, it may be possible to model the effect of particle breakup on the results when f is assumed to be a function of particle size.

Acknowledgments

The authors acknowledge the helpful discussions with Drs. M. R. Baer and J. W. Nunziato, Sandia National Laboratories, who suggested to us that the problem could be addressed in the limits we have studied. We also acknowledge the assistance of Mr. Mark Miller, graduate student, M/IE, University of Illinois at Urbana-Champaign.

References

Baer, M. R., 1988, "Numerical Studies of Dynamic Compaction of Inert and Energetic Granular Materials," ASME JOURNAL OF APPLIED MECHANICS, Vol. 55, pp. 36–43.

Baer, M. R., and Nunziato, J. W., 1986, "A Two-Phase Mixture Theory for the Deflagration-to-Detonation Transition (DDT) in Reactive Granular Materials," *Int. J. Mulitphase Flow*, Vol. 12, pp. 861–889.

Bdzil, J. B., Engelke, R., and Christenson, D. A., 1981, "Kinetics Study of a Condensed Detonating Explosive," *J. Chem. Phys.*, Vol. 74, pp. 5694–5699.

Becker, E., and Bohme, G., 1969, "Steady One-Dimensional Flow; Structure of Compression Waves," *Nonequilibrium Flows*, P. P. Wegener, ed., Marcel Dekker, New York.

Bernecker, R. R., and Price, D., 1974, "Studies in the Transition from Deflagration to Detonation in Granular Explosives—I. Experimental Arrangement and Behavior of Explosives Which Fail to Exhibit Detonation," *Combust. Flame*, Vol. 22, pp. 111–118.

Bernecker, R. R., and Price, D., 1974, "Studies in the Transition from Deflagration to Detonation in Granular Explosives—II. Transitional Characteristics and Mechanisms Observed in 91/9 RDX/wax," *Combust. Flame*, Vol. 22, pp. 119–129.

Butcher, B. M., Carroll, M. M., and Holt, A. C., 1974, "Shock-Wave Compaction of Porous Aluminum," *J. Appl. Phys.*, Vol. 45, pp. 3864–3875.

Butler, P. B., and Krier, H., 1986, "Analysis of Deflagration to Detonation Transition in High-Energy Solid Propellants," *Combust. Flame*, Vol. 63, pp. 31–48.

Butler, P. B., Lembeck, M. F., and Krier, H., 1982, "Modeling of Shock Development and Transition to Detonation Initiated by Burning in Porous Propellant Beds," *Combust. Flame*, Vol. 46, pp. 75–93.

Carroll, M. M., and Holt, A. C., 1972, "Static and Dynamic Pore-Collapse Relations for Ductile Porous Materials," *J. Applied Physics*, Vol. 43, pp. 1626–1635.

Elban, W. L., and Chiarito, M. A., 1986, "Quasi-Static Compaction Study of Coarse HMX Explosive," *Powder Technology*, Vol. 46, pp. 181–193.

Elban, W. L., Coyne, P. J., and Chiarito, M. A., 1987, "The Effect of Particle Size on the Quasi-Static Compaction Behavior of Granular HMX Beds," 1987 JANNAF Propulsion Systems Hazards Subcommittee Meeting, CPIA Publication 464, pp. 61–75.

Gokhale, S. S., and Krier, H., 1982, "Modeling of Unsteady Two-Phase Reactive Flow in Porous Beds of Propellant," *Prog. Energy Combust. Sci.*, Vol. 8, pp. 1–39.

Kooker, D. E., 1986, "A Numerical Study of Compaction Waves in Class D HMX, 1986 JANNAF Propulsion Systems Hazards Subcommittee Meeting, CPIA Publication 446, Vol. 1, pp. 213–238.

Kooker, D. E., 1987, "A Workshop Summary of Compaction Waves in Granular Material: Numerical Predictions," 1987 JANNAF Propulsion Systems Hazards Subcommittee Meeting, CPIA Publication 464, Vol. 1, pp. 127–138.

Krier, H., and Stewart, J. R., 1985, "Prediction of Detonation Transition in Porous Explosives from Rapid Compression Loadings," UILU-ENG-85-4007, Department of Mechanical and Industrial Engineering, Univ. of Illinois at Urbana-Champaign.

Lyczkowski, R. W., Gidaspow, D., Solbrig, C., and Hughes, E. D., 1978, "Characteristics and Stability Analyses of Transient One-Dimensional Two-Phase Flow Equations and Their Finite Difference Approximations," *Nuclear Science and Engineering*, Vol. 66, pp. 378–396.

Marsh, S. P., ed., 1980, *LASL Shock Hugoniot Data*, University of California Press, Berkeley, CA.

Powers, J. M., Stewart, D. S., and Krier, H., 1987, "Two-Phase Steady Detonation Analysis," presented at the 11th International Colloquium on Dynamics of Explosions and Reactive Systems, Warsaw, Poland, to appear in AIAA Progress Series.

Powers, J. M., 1988, "Theroy of Detonation Structure for Two-Phase Materials," Ph.D. Dissertation, Univ. of Illinois at Urbana-Champaign.

Price, D., and Bernecker, R. R., 1975, "Sensitivity of Porous Explosives to Transition from Deflagration to Detonation," *Combust. Flame*, Vol. 25, pp. 91–100.

Sandusky, H. W., and Bernecker, R. R., 1985, "Compressive Reaction in Porous Beds of Energetic Materials," *Proceedings-Eighth Symposium (International) on Detonation*, NSWC MP 86-194, Naval Surface Weapons Center, White Oak, Md., pp. 881–891.

Sandusky, H. W., and Liddiard, T. P., 1985, "Dynamic Compaction of Porous Beds," NSWC TR 83-256, Naval Surface Weapons Center, White Oak, Md.